An alternative method for gas temperature determination in nitrogen plasmas: Fits of the bands of the first positive system ($B\ ^3\Pi_g \rightarrow A\ ^3\Sigma_u^+$)

Costel Biloiu,[a] Xuan Sun, Zane Harvey, and Earl Scime
Physics Department, West Virginia University, Morgantown, West Virginia 26506

(Received 1 April 2006; accepted 31 December 2006; published online 4 April 2007)

A method of gas temperature determination in nitrogen or nitrogen doped discharges is presented. The method employs fits of numerically generated spectra of the 0-0, 1-0, and 2-0 bands of the first positive system ($B\ ^3\Pi_g \rightarrow A\ ^3\Sigma_u^+$) of nitrogen to experimental measurements. Excellent agreement between gas temperature values inferred by using this method and by using the 3-0 band peak ratio method [M. Simek and S. De Benedictis, Plasma Chem. Plasma Proc. **15**, 451 (1995)] is demonstrated for a helicon plasma. The spectral model is available for use by the plasma spectroscopy community. The model, along with user instructions, can be downloaded from Electronic Physics Auxiliary Publication Service of American Institute of Physics. The model includes the line positions, Hönl-London factors, and provides rapid determination of gas temperature if one or more of the aforementioned emission rovibrational band spectra are available.
 [DOI: 10.1063/1.2537448]

I. INTRODUCTION

Besides plasma density, electron temperature, and ion energy, the neutral gas temperature (T_g) is another important parameter for plasma processing in reactive gases. In plasma enhanced chemical vapor deposition, the chemistry of the discharge can be influenced by the gas temperature since it governs the reaction rate of active species generation through dissociation, excitation, and ionization processes. Moreover, the deposited film uniformity as well as intrinsic film properties, especially for large area reactors, can be affected by gas temperature gradients in the proximity of the substrate since T_g is intimately connected with the density and the flux of the heavy species. Similarly, for plasma etching, gas temperature gradients above the wafer surface may lead to neutral density nonuniformities accompanied by different etching yields and variable etching anisotropy over the wafer surface. Therefore, accurate knowledge of the gas temperature is required to understand and control plasma processes.

There are many applications of nitrogen or nitrogen containing plasmas such as oxynitride and silicon nitride film deposition,[1] hard materials synthesis,[2] surface hardening by plasma immersion ion implantation,[3] and plasma-assisted molecular beam epitaxy of III-V nitride semiconductors.[4] These applications employ many types of electrical discharges that span wide ranges of gas pressure and input power. Since N_2 molecules exchange rotational and translational energy faster with heavy particles than with electrons, it is possible that rotational distributions quickly achieve thermodynamic equilibrium with the bulk gas. Therefore, for these plasmas a convenient way to determine T_g is through the measurement of the rovibrational band spectrum of nitrogen. Even for plasmas that do not contain nitrogen, the rovibrational band spectrum of nitrogen can be used as a sensitive "thermometer" for the gas temperature by the addition of trace amounts of N_2, i.e., a molecular actinometer. Due to its simplicity and high sensitivity, optical emission spectroscopy (OES) is the most common way to determine the gas temperature for different types of discharges and a wide range of working conditions (see Table I). Usually, different bands of the first negative system (1^-) of N_2^+ ($B\ ^2\Sigma_u^+ \rightarrow X\ ^2\Sigma_g^+$) (Refs. 5–11) and the second positive system (2^+) of N_2 ($C\ ^3\Pi_u \rightarrow B\ ^3\Pi_g$) (Refs. 8–16) are used either through a Boltzmann plot when the resolution of the employed spectrometer is high enough to resolve the rotational structure of the bands or by fitting numerical models to the band envelope when medium and low resolution spectrometers are used. However, as pointed out by Cruden *et al.*,[17] the rotational temperature is a correct measure of the translational temperature of neutral gas species only if certain conditions are fulfilled: (i) The emitting rotational level distribution is in thermal equilibrium, i.e., it obeys a Boltzmann distribution; (ii) the gas temperature is high enough to equilibrate between translational and rotational degrees of freedom; (iii) there is an equilibrium between the rotational temperature of the emitting electronic state and the ground level electronic state; and (iv) there is an equilibrium between the rotational temperatures of different excited species that are present in the discharge.

In high pressure and/or high power density discharges, local thermodynamic equilibrium (LTE) typically occurs and the aforementioned conditions are fulfilled. However, the low pressure discharges often employed in plasma processing are far from LTE. Thus, OES measurements of rotational temperature in low pressure discharges are problematic and it is possible that the inferred rotational temperatures do not represent the true gas temperature. Even so, the rotational temperature may still be a good indicator of the gas temperature if the excited rotational state is populated by transitions directly from the molecular ground state. If multiple pathways compete in populating the emitting rotational state,

[a]Author to whom correspondence should be addressed; electronic mail: costel.biloiu@mail.vsea.com; at present with Varian Semiconductor Equipment Associates, Gloucester, MA 01966

TABLE I. Gas temperature in plasmas of pure N_2 and mixtures of N_2 under different experimental conditions obtained by employing different estimation methods.

Discharge type	Gas/flow rate	Pressure (Torr)	Power density/input power[a]	Method(s)[b]	Temperature (K)	Ref.
0.5–2.5 A dc magnetron	N_2/20 sccm	$\sim 1\times10^{-3}$	1–6 mW/cm^3	1^- fit	400±30	5
13.56 MHz inductively coupled	N_2	1×10^{-3}	0.2 and 15 mW/cm^3	1^+ LAS	330–460	23
0.46 MHz inductively coupled	N_2/60 sccm	$1-15\times10^{-3}$	2 and 10 mW/cm^3	2^+ fit 1^- fit	450–580 940–1140	10
13.56 MHz inductively coupled	N_2	50×10^{-3}	0.17–0.85 W/cm^3 [c]	1^- EBF	315–380	22
55 kHz ac glow	N_2/25 sccm	1	0.25 W/cm^3 and 0.6 W/cm^3	1^- and 2^+ fit 1^- LIF	450–530	11
433 MHz microwave	N_2/1500 sccm	~3.3	300 W	1^+ LAS and DB	945±50[d]	24
Plasma torch	N_2	3650	-	1^- and 2^+ fit 1^- BP	4400±400	8
200 kHz pulsed magnetron	70% Ar+15% O_2+15% N_2	3×10^{-3}	100–700 W 80 mm gap	1^- fit	370–520	7
Inductively amplified dc magnetron	Ar+20% N_2	30×10^{-3}	100–1500 W 6 cm above target	1^+ fit	300–700	46
13.56 MHz inductively coupled	Cl_2+(2–5)% N_2/20–175 sccm	$2-20\times10^{-3}$	0.36 W/cm^3	2^+ fit	650–1250	12
55 kHz ac glow	CCl_4+2% N_2/10 sccm	155×10^{-3}	0.7 W/cm^3	2^+ fit CCl LIF	500–680 385–620	11
1.8–2.2 MHz inductively coupled	Ar, He, Ne, O_2+(5–10)% N_2	$20-700\times10^{-3}$	2–7 W/cm^3	2^+ fit	600–2500	13
27 MHz capacitively coupled	He+5% N_2	200×10^{-3}	~0.14 W/cm^3	1^+ PR and 1^+ LIF	350±40	25
dc glow	Variable Ar/N_2/100 sccm	~1	0.03–0.15 W/cm^3	1^- fit	400–700	7
400 kHz transformer coupled	Ar+C_2F_6+O_2+9% N_2	2.5	17.4 W/cm^3	2^+ fit	5500±230	14
825 MHz microwave	99.9%Ar+0.1% N_2	10–40	0.3–0.7 W	2^+ fit	350–370	15
19.7 kHz dielectric barrier	Ar+(5–10)% N_2	320–1200	1 W 0.15 cm gap	1^- BP	400–600	6
50 Hz gliding arc	Air	760	1.3 kW few mm gap	1^- and 2^+ fit	2300±200	9
Liquid nonmetallic electrodes dc	Air	760	150 W 6–8 mm gap	2^+ fit	2500±200[e]	16

[a]Reported or calculated values based on reported input power and discharge geometry data; where such data were not available, the input power and/or interelectrode gap are given.
[b]1^-, 1^+, and 2^+ stand for the first negative, the first positive, and the second positive systems, respectively (see Fig. 1); LAS: laser absorption spectroscopy, EBF: electron beam fluorescence, LIF: laser induced fluorescence, PR: peak ratio, BP: Boltzmann plot, DB: Doppler broadening.
[c]Calculated values taking into account the plasma source volume; if the expansion chamber is to be taken into account then a power density of ~15.6 mW/cm^3 will result.
[d]The value in the active discharge zone inferred from Boltzmann plot; as reported, Doppler broadening method gave ~250 K higher temperature; in the short-lived afterglow both methods gave ~530 K.
[e]Value at the approximately half distance between electrodes; otherwise, ~1900 K and ~900 K in the proximity of the cathode and anode, respectively.

multiple rotational temperatures corresponding to the different excitation pathways may contribute to the emission spectrum of the state. By using a fitting procedure based on two Boltzmann distributions, Linss *et al.*[7] reported two rotational temperatures for the case of the 0-0 band of the first negative system: A "cold" distribution of 440 K which was the true gas temperature and a "hotter" distribution of 2460 K. These temperatures corresponded to two different excitation channels of the $N_2^+(B\ ^2\Sigma_1^+)$ state (see Fig. 1): The first channel was excitation through electron impact directly from the ground state of the neutral molecule or stepwise via ionization and subsequent excitation and the second channel was vibrational energy transfer through collisions between the ground state ion $N_2^+(X\ ^2\Sigma_g^+)$ and the high vibrational level ($v \geq 12$) ground state molecule $N_2(X\ ^1\Sigma_g^+)$. Similarly, using emission spectra from 0-0 band of the 1^- system in an experiment with external gas temperature control, Goyette *et al.*[18] reported a ~150 K higher temperature for T_g inferred from a Boltz-

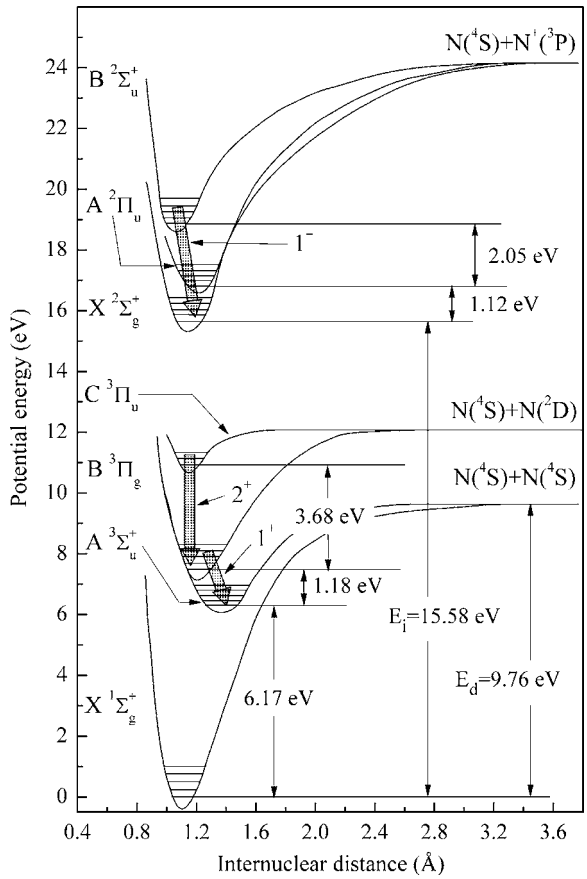

FIG. 1. Simplified energetic diagram of N_2 (adapted from Ref. 26) showing different molecular, ionic, and atomic states as well as principal radiative decay channels employed in gas temperature estimation.

mann plot of the *R*-branch lines than the externally imposed temperature. They also reported that good agreement between the gas kinetic temperature and the inferred temperature was obtained only for the 2-0 band in the case of the 2^+ system when using an experimentally measured band profile parameter (the ratio of the first minimum to the secondary minimum) for rotational temperature estimation. Inaccurate determination of the gas temperature using emission from the 3-1 and 4-1 bands was attributed to the presence of additional emission superposed on these bands that prevented an accurate assessment of the band profile parameter. Golubovskii and Telezhko[19] have shown that excitation through the neighboring metastable $E\ ^3\Sigma_u^+$ state may cause significant perturbation of the rotational distribution of the $C\ ^3\Pi_u$ state and consequently considerable errors can arise in determination of the gas temperature by using the 2^+ system. Moreover, the use of the 2^+ system in N_2/Ar mixtures is problematic due to the presence of Ar ($^3P_2$) and Ar ($^3P_0$) metastable states that can lead to perturbations of the rotational distributions of low lying $C\ ^3\Pi_u$ state vibrational levels through resonant energy transfer (the metastable state energies of 11.55 and 11.72 eV, respectively, lie within the energy range of $v=0-4$ vibrational levels). However, due to its simplicity and population mechanism mainly by electron impact from ground state, the N_2 2^+ system remains the most widely used band system in gas temperature estimation.

Nonequilibrium between the rotational temperature and the gas temperature and/or population mechanisms other than electron impact excitation from the ground state can lead to overestimation of the true gas temperature. However, if an appropriate coronal[20] or collisional radiative model is available, the gas temperature can be inferred by comparing the measured rotational temperature to the value predicted by the model for a given gas temperature and related plasma parameters. Lavrov *et al.*[21] have shown that the rotational temperature inferred from the rotational distribution of an emitting state is equal to the gas temperature only when the characteristic rotation-translation relaxation time is much smaller than that of the primary deexcitation process, i.e., the radiative lifetime. Therefore, under plasma conditions for which vibrational states do not satisfy the relaxation time condition, OES cannot be used for gas temperature determination. In such cases, more sophisticated methods such as electron beam fluorescence, laser induced fluorescence, laser absorption spectroscopy, or Doppler-resolved spectroscopy must be employed to obtain accurate gas temperatures. In these four methods, the gas temperature is inferred by interrogation of the molecule ground state $X\ ^1\Sigma_g^+$,[22] the ion ground state $X\ ^2\Sigma_g^+$,[11] or a low lying $A\ ^3\Sigma_u^+$ metastable state,[23–25] where the ion ground state and the low lying molecule metastable state are directly collisionally coupled to the molecule ground state.

In this work, we present a method of gas temperature determination that employs a fit of numerically generated spectra to the 0-0, 1-0, and 2-0 emission bands of the first positive (1^+) system of N_2 ($B^3\Pi_g \rightarrow A^3\Sigma_u^+$). The method proposed here is intended to be a tool for the plasma spectroscopy community for determination of the gas temperature in nitrogen or nitrogen doped discharges. The fitting code along with line positions and intensities is available electronically and can be downloaded either from Electronic Physics Auxiliary Publication Service (EPAPS) of the American Institute of Physics or from our laboratory webpage.

II. STRUCTURE OF THE N_2 FIRST POSITIVE SYSTEM

The first positive system (1^+) is perhaps the most accessible band system of nitrogen. It includes multiple-headed bands degraded to shorter wavelength and extends from the near infrared to the blue.[26] As shown schematically in Fig. 1, bands composing this system correspond to transitions between different vibrational levels of the $B\ ^3\Pi_g$ and $A\ ^3\Sigma_u^+$ electronic states. For the upper state, the spin-orbit constant $\mathbb{A}_{v'}$ for $v'=0-2$ is roughly equal to 42 cm^{-1} whereas the rotational constant $B_{v'}$ varies between 1.63 and 1.59 cm^{-1}, yielding a $Y=\mathbb{A}_{v'}/B_{v'}$ parameter of ~ 26. Therefore, with a good approximation, for low J' values the $B\ ^3\Pi_g$ state may be treated as belonging to Hund's case (a).[27] However, as J' increases the $Y \gg J'$ condition is no longer fulfilled and the *B* state should be treated as belonging to an intermediate case between Hund's case (a) and (b). Hence, the *B* state consists of six electronic substates $^3\Pi_{\Omega g}^{e,f}$, with $\Omega=\Lambda+\Sigma$ (the sum of orbital quantum number Λ and the Hund's case (a) quantum number for the component of the spin on internuclear axis Σ) $=0$, 1, and 2, and e/f denotes the parity of the states.[28] Having $\mathbb{A}_{v''}=0$, the lower electronic state, $A\ ^3\Sigma_u^+$, belongs to

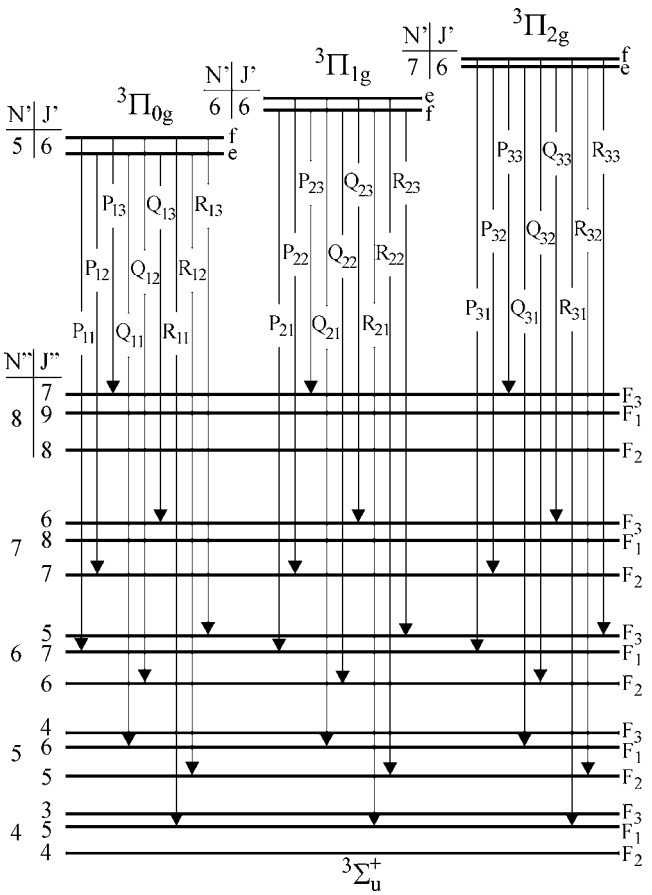

FIG. 2. The *P*, *Q*, and *R* branch structures of the N_2 first positive band system for Hund's case (a).

Hund's case (b). As shown in Fig. 2, the complex structure of the band system arises from the separation of the $^3\Pi_\Omega$ manifolds which gives rise to three sub-bands $^3\Pi_{0g}\rightarrow{}^3\Sigma_u^+$, $^3\Pi_{1g}\rightarrow{}^3\Sigma_u^+$, and $^3\Pi_{2g}\rightarrow{}^3\Sigma_u^+$. Furthermore, each sub-band has 9 branches denoted *P*, *Q*, and *R* that correspond to $\Delta J=-1$, 0, and +1, respectively, with different intensities (branches having $\Delta J=\Delta N$, where *N* is the Hund's case (b) quantum number, are strong; branches having $\Delta J=\Delta N\pm1$ are medium; and branches having $\Delta J=\Delta N\pm2$ are weak) and therefore contribute differently to the band profile shape.

In a nitrogen plasma, the upper $B\ ^3\Pi_g$ state is a result of balance between many excitation and quenching process such as electron impact excitation from the molecule ground state $X\ ^1\Sigma_g^+$ and first metastable state $A\ ^3\Sigma_u^+$; associative excitation $X\ ^1\Sigma_g^+ + A\ ^3\Sigma_u^+$; pooling reactions of the $A\ ^3\Sigma_u^+$ state; atom recombination $N(^4S)+N(^4S)$; radiative decay of the $C\ ^3\Pi_u$ state; intersystem collisional transfer of energy between the $A\ ^3\Sigma_u^+$, $B\ ^3\Pi_g$, $W\ ^3\Delta_u$, and $B'\ ^3\Sigma_u^-$ states; quenching by collisions with molecules; and radiative decay.[29] The low threshold (7.35 eV) of the electron excitation cross section for the 1^+ system (a maximum of $\sim0.3\times10^{-16}$ cm^2 at 12 eV),[30] which, for the electron temperatures of a few electron volts usually encountered in low temperature plasmas, yields excitation rate coefficients of $\sim2\times10^{-9}$ cm^3/s,[31–33] and makes the electron impact excitation from the molecule ground state the main channel for population of this state in most low pressure discharges.[34] For example, using the steady-state portion of the nitrogen plasma kinetic model developed by De Benedictis *et al.*,[29] in a 100 mTorr discharge in pure nitrogen with a gas temperature of 350 K, an electron temperature of $\sim1-2$ eV, and an electron density of 4×10^{10} cm^{-3}, the production rate of the $B\ ^3\Pi_g$ state by electron impact from the molecule ground state is 1.85×10^{14} cm^{-3} s^{-1}, approximately 55% of the total production rate. The next most significant population process is electron impact excitation from the metastable $A\ ^3\Sigma_u^+$ state, which accounts for ~34% of the total production rate. Other processes that contribute to the population of the $B\ ^3\Pi_g$ state are ~7%—the radiative decay of the upper $C\ ^3\Pi_u$ state, ~3%—the associative excitation, and ~1%—the pooling reaction of the $A\ ^3\Sigma_u^+$. Consequently, for such plasma conditions, the first positive system will provide a more accurate representation of the molecule ground state than the 1^- or 2^+ systems because the main population channels are electron impact excitation from the molecule ground state and from the low lying $A\ ^3\Sigma_u^+$ metastable state. As laser absorption spectroscopy[23,24] and laser induced fluorescence[25] investigations have demonstrated, due to its long radiative lifetime (~1.9 s) (Ref. 26) the rotational distribution of $A\ ^3\Sigma_u^+$ state is fully thermalized.

Another advantage of using the 1^+ system in low pressure plasmas is the longer radiative lifetime of the *B* state ($12-14\ \mu$s for $v=0-12$),[35] which favors rotational-translational equilibration at pressures as low as a few tens of millitorr. For example, consider the collisional relaxation of N_2 molecules in plasmas with gas temperatures below 1000 K. Using an exponential extrapolation of the average cross section for the momentum transfer given by Phelps[36] for gas temperatures below 1000 K, the mean gas-kinetic collision time[37] of N_2 molecules may be written as

$$\bar{t}_c = 17.7\sqrt{T_g}/\{p[1+2.14\exp(-6\times10^{-4}\ T_g)]\}, \qquad (1)$$

with temperature in K, pressure in Torr, and collision time in nanoseconds. Equation (1) yields a mean neutral collision time on the order of 11 μs at 10 mTorr and 300 K, much longer than the radiative lifetimes of ~40 ns for the $N_2\ (C\ ^3\Pi_u)$ state[38] and ~60 ns for the $N_2^+(B\ ^2\Sigma_u^+)$ state.[26] Therefore, thermalization of the rotational distributions of these states is not possible before the levels decay radiatively. Assuming that the $N_2(B\ ^3\Pi_u)$ state rotational distribution requires 2–3 collisions before being thermalized, the lower pressure limit for which conditions (i)–(iv) are fulfilled is about 20–30 mTorr. A similar calculation for $N_2\ (C\ ^3\Pi_u)$ and $N_2^+(B\ ^2\Sigma_u^+)$ gives a low pressure limit of 825 and 550 mTorr, respectively. The quenching rate coefficients of $N_2(B\ ^3\Pi_g)$ by normal nitrogen molecules are $1-8\times10^{-11}$ cm^3 s^{-1} for $v=1-12$.[39] A simple estimate shows that for the 20–30 mTorr low pressure limit, the characteristic time of the quenching process which is the other channel that compete to the deactivation of the $N_2(B\ ^3\Pi_g)$ state is roughly one order of magnitude longer than rotational-translation relaxation time.

Other advantages of the 1^+ system over the 1^- and 2^+ systems include: high emission intensity under most discharge conditions that provides for good detection even in afterglow plasma (a roughly three orders of magnitude higher population in the low lying $v=0-2$ vibrational levels

of the B state than in the corresponding vibrational levels of the C state has been reported for a 40–700 mTorr, 100 W input power, 27.12 MHz capacitively coupled N_2 discharge),[40] higher energy predissociation level [$v=12$, $J=33$ (Ref. 41) compared with $v=2$, $J=55$; $v=3$, $J=43$; $v=4$, and $J=28$ for the 2^+ system[26]], and minimal perturbations by neighboring states,[42] which results in undistorted rotational distributions; and for the bands chosen in these experiments, a lack of overlap with bands from the same sequence (being the first bands in their sequences the overlapping is negligible), or bands from other sequences or systems (the first overlap occurs between the 4-0 and 12-9 bands at 618.52 nm; the Hermann's infrared system and infrared afterglow system are too weak compared to 1^+ system to cause problems; and the relatively strong $\Delta v=1$ sequence of Meinel's auroral system is in the range 920–950 nm),[35] or bright atomic lines [the strong atomic triplet ($3s\ ^4P-3p\ ^4S^0$), septet ($3s\ ^4P-3p\ ^4P^0$), quartet ($3s\ ^2P-3p\ ^2P^0$), and octet ($3s\ ^2P-3p\ ^4D^0$) transition arrays[43] are in the 742.4–746.8, 818.5–824.2, 856.8–865.5, and 868.0–872.8 spectral regions].[44] However, the complex structure of the 1^+ system has prevented the widespread use of the 1^+ band system in gas temperature estimation. We are aware of four reports in which OES of the 1^+ system was used for gas temperature determination. Golubovskii and Telezhko[19] used a technique involving the creation of a band profile parameter, the slope of the third sub-bandhead intensity versus wavelength curve normalized to its amplitude, for the unresolved 12-8 band. We note that in the English translation of their paper there is an obvious typographical error. The pressure range for their work is not 0.01–13 GPa, but 1–500 Pa as shown in their Fig. 3. Using their band profile method they found 10%–15% lower temeperature values than values inferred from 0-2 band of the N_2 2^+ system even after accounting for a 3% hot population. They argued that measurement of the gas temperature from the 1^+ system is more accurate than from the 2^+ system because of the favorable combination of rotational-translation relaxation times, radiative decay times, and quenching times of the B state. Piper *et al.*[35] used a fit of the entire 1^+ band system to calculate the Einstein transition probabilities of the $B\ ^3\Pi_g$ state and also addressed the problem of bands overlap. Simek and De Benedictis[45] proposed a handy method based on ratios of the second and third peaks to the intensity of 3-0 band head. Their technique was effective for instrument resolutions better than 2 Å and gas temperatures less than 1000 K. Ricard *et al.*,[46] fit a model function to the 2-0 band to determine the gas temperature. Temperatures between 300 and 700 K for input powers up to 1.5 kW in an inductively amplified magnetron discharge were reported, but no details of the fitting procedure were provided.

III. THE SPECTRAL MODEL

A. Line positions

A synthetic spectrum of a rovibrational band can be generated if the individual rotational line positions and intensities are known. Budo's formulas[47] and Dunham series[48] for calculation of $B\ ^3\Pi_g$ and $A\ ^3\Sigma_u^+$ triplet terms, even after corrections for spin-orbit interaction and centrifugal motion, lack sufficient precision, particularly at higher J values, for comparison with experimental observations. The average uncertainty in calculated line positions for $J>20$ is on the order of $0.5\ \mathrm{cm}^{-1}$. Such uncertainties correspond to only ~0.04 nm in terms of wavelength, but because of the close spacing of the rotational lines the simulated spectra cannot reproduce the characteristic features of precisely measured spectra and therefore lead to erroneous temperature estimations. In the model described in this work, we use line positions calculated and experimentally verified by Effantin *et al.*[49] The calculations were based on diagonalization of effective Hamiltonians and the experimental verification accomplished by comparison with high resolution spectra obtained with a Fourier transform interferometer from a 10 Torr, electrodless, fused silica lamp N_2 discharge. The uncertainty in line positions was less than $0.007\ \mathrm{cm}^{-1}$. For use with our measured spectra, the line positions were converted into air wavelengths by multiplying with the refraction index of air given by[50]

$$10^8(n_a-1)=c_1/(c_2-\tilde{\nu}^2)+c_3/(c_4-\tilde{\nu}^2), \tag{2}$$

where $\tilde{\nu}$ is the wave number in $\mu\mathrm{m}^{-1}$ and c_1-c_4 are constants equal to 572 105, 238.018 5, 167 917, and 57.362 $\mu\mathrm{m}^{-2}$, respectively.

B. Line intensities

The emission intensity of an individual rotational line between two levels having electronic, vibrational, and rotational quantum numbers n, v, and J is given by

$$I^{n'v'J'}_{n''v''J''}=N_{n'v'J'}A^{n'v'J'}_{n''v''J''}\frac{hc}{\lambda}, \tag{3}$$

where the first prime ($'$) and the second prime ($''$) denotes the upper and lower levels, respectively, $N_{n'v'J'}$ is the population of the emitting level, $A^{n'v'J'}_{n''v''J''}$ is the Einstein transition probability, λ is the wavelength of the emitted radiation, h is Planck's constant, and c the speed of light. With the normalization condition[51] of the Hönl-London factors the transition probability may be written as[27]

$$A^{n'v'J'}_{n''v''J''}=\frac{A^{n'v'}_{n''v''}S_{J'J''}}{(2-\delta_{0,\Lambda})(2S+1)(2J'+1)}, \tag{4}$$

where $S_{J'J''}$ is the Hönl-London factor for the considered transition, $\delta_{0,\Lambda}$ is the Kronecker delta (equal to 1 if $\Lambda=0$ and 0 for all other values), $2S+1$ is the spin multiplicity, J' is the upper level rotational quantum number, and $A^{n'v'}_{n''v''}$ is the band strength or the band transition probability given by[52]

$$A^{n'v'}_{n''v''}=\frac{64\pi^4}{3h\lambda^3}q_{v'v''}|R_e(\bar{r}_{v'v''})|^2, \tag{5}$$

where $q_{v'v''}$ is the Franck-Condon factor of the $v'\rightarrow v''$ band and $|R_e(\bar{r}_{v'v''})|^2$ is the square of the electronic-vibrational transition moment.

Under the assumption of Hund's case (a), the population of the upper level may be written as[53]

$$N_{n'v'J'} = N \times \frac{2\Phi_{J'}(2S+1)(2J'+1)}{S} \frac{1}{Q_{\mathrm{el}}Q_{\mathrm{vib}}Q_{\mathrm{rot}}} \sum_{\Sigma=-S} [-(hc/k_BT)\mathbb{A}_{v'}\Lambda\Sigma] \times \exp\{-(hc/k_BT)[T_{\mathrm{el}} + G_{\mathrm{vib}}(v') + \mathbb{A}_{v'}\Lambda\Sigma + F_{\mathrm{rot}}(J')]\}, \quad (6)$$

where T_{el}, $G_{\mathrm{vib}}(v')$, $F_{\mathrm{rot}}(J')$, Q_{el}, Q_{vib}, and Q_{rot} are electronic, vibrational, and rotational spectral terms and partition functions, respectively, N is the entire population of the upper electronic level, and $\Phi_{J'}$ is an alternation factor which is a function of nuclear spin I and takes into account the parity of the rotational level. For homonuclear molecules its value is $(I+1)/(2I+1)$ for symmetric levels and $I/(2I+1)$ for asymmetric levels.[53] In the case of the N_2 molecule, $I=1$ and thus $\Phi_{J'}=2/3$ or 1/3 for symmetric and asymmetric levels, respectively. Taking into account the alternation of symmetric and asymmetric levels (see Fig. 2) for Hund's case (a), it implies double the intensity for e and f levels having even and odd J', respectively. Since for a given $v' \rightarrow v''$ band of the $B \rightarrow A$ system, $A^{n'v'}_{n''v''}$ from Eq. (5) and T_{el}, $G_{\mathrm{vib}}(v')$, Q_{el}, Q_{vib}, and the sum from denominator from Eq.(6) are constant, the intensity of a recorded line originating from the same electronic and vibrational level may be written as

$$I^{Bv'J'}_{Av''J''} = \mathrm{const.} \times \frac{S(\lambda)\Phi_{J'}S_{J'J''}}{T\lambda^4} \times \exp\{-(hc/k_BT)[\mathbb{A}_{v'}\Lambda\Sigma + B_{v'}J'(J'+1)]\}, \quad (7)$$

where $S(\lambda)$ is the overall optical path sensitivity [windows, collection optics, optical fiber, spectrometer, and charge-coupled camera (CCD) camera], Q_{rot} has been replaced by $k_BT/hcB_{v'}$ (which is valid for gas temperatures above room temperature), and $F_{\mathrm{rot}}(J')$ has been replaced by $B_{v'}J'(J'+1)$ (which is valid for low J' values). For higher J' values, centrifugal, spin-rotation, and spin-spin corrections may be added into rotational term but generally these corrections are very small.[54] For example, for the 2-0 band and $J'=40$, the centrifugal correction $D_{v'}[J'(J'+1)]^2$ accounts for only 0.6% of the rotational term (see Table II). Writing all the energy terms in cm^{-1} and $hc/k_B=1.44$ cm K, the temperature in Eq. (6) is in Kelvin. In calculating the line intensities, we computed the Hönl-London factors using the formulas given by Kovacs[54] for triplet transitions in the intermediate regime between Hund's case (a) and case (b). The relevant constants were calculated from the equilibrium molecular constants of the $B\ ^3\Pi_g$ and $A\ ^3\Sigma^+_u$ states tabulated by Roux *et al.*[55] (see Table II). As shown in Fig. 3, for higher J' (>10) only branches $(P,Q,R)_{ij}$ having $i=j$ $(\Delta J=\Delta N)$ contribute significantly to the band profile shape.

C. Synthetic spectrum generation

Using the line positions and intensities as described above, an emission spectrum including all 27 branches and J values from zero to a maximum value can be generated numerically for any given gas temperature. In our model, we stop at $J'=40$. As shown in Fig. 4, lines originating from $J'>40$ contribute to the details of the band tail and neglecting them does not significantly affect the main features of the band spectrum. Before comparison with the observations, each line is convolved with an apparatus function. To model the instrumental broadening, we use a pseudo-Voight function, i.e., a combination of a Gaussian and a Lorentzian function

$$f(p,w) = p\frac{\sqrt{4\ln 2}}{\sqrt{\pi}w}\exp\left[-\frac{4\ln 2}{w^2}(\lambda-\lambda_0)^2\right] + (1-p)\frac{2}{\pi}\cdot\frac{w}{w^2+4(\lambda-\lambda_0)^2}, \quad (8)$$

where p and $1-p$ are the relative magnitudes of the Gaussian and Lorentzian functions contributions, respectively, w is the full width at half maximum of the line (FWHM), and λ_0 is the central wavelength. Parameters p and w may be experimentally determined by measuring the shape of an atomic line from a low temperature spectral source with the same optical path used for the N_2 observations (see Fig. 5). Since the apparatus function varies as a function of wavelength for a fixed slit width, calibration of spectral lines in the wavelength range of interest are needed for each emission band (between the band head and the tail of the band). We used Ar I lines from an argon pen lamp and the experimentally determined apparatus function parameters at each wavelength are summarized in Table III.

Determination of the rotational temperature was automated in MATLAB™ with a nonlinear chi-squared minimization, i.e.,

$$\chi^2(T) = \left\{\sum_{k=1}^{Z}[I^r_k - I^s_k(T)]^2\right\}/[Z(Z-1)], \quad (9)$$

where I^s_k is the simulated spectrum and Z is the number of points in the recorded spectrum. I^r_k is the raw experimental spectrum corrected for the spectral sensitivity of the optical path, with background subtracted, and normalized to the band head intensity. As will be shown, since the intensity is

TABLE II. Molecular constants for the 0-0, 1-0, and 2-0 emission bands of the 1^+ system.

Rotational band	Band head position[a] λ_{air} (nm)	Spin-orbit constant[b] $\mathbb{A}_v$ (cm^{-1})	Rotational constant[b] B_v (cm^{-1})	Centrifugal constant[b] $D_v\times10^5$ (cm^{-1})
0→0	1051.00	42.23111	1.62881	0.58553
1→0	891.24	42.18482	1.61057	0.58877
2→0	775.32	42.13472	1.59223	0.59225

[a]Taken from Ref. 26.
[b]Calculated according to: $\mathbb{A}_v, B_v, D_v = \mathbb{A}_e, B_e, D_e - a_{A,B,D}(v'+1/2) + \beta_{A,B,D}(v'+1/2)^2 + \gamma_{A,B,D}(v'+1/2)^3 + \cdots$, where $\mathbb{A}_e$, B_e, D_e, α, β, and γ are N_2 equilibrium molecular constants taken from Ref. 55.

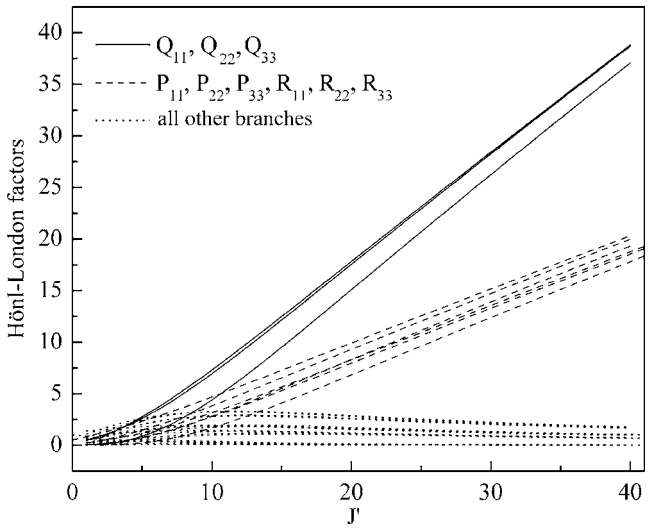

FIG. 3. Calculated Hönl-London factors of the 1-0 band of the N_2 first positive system for intermediate case between Hund's case (a) and (b).

normalized to the band head intensity and the band head is composed of lines of P_{11}, Q_{12}, and R_{13} branches with low J', this technique is sensitive to small changes in the gas temperature. The MATLAB™ code allows users to choose the band to be fit (the 0-0, 1-0, and 2-0 bands), to input the apparatus function parameters p and w, the maximum value of J to use in the simulated spectrum, and to adjust the absolute wavelength of the measured spectrum in case of a small wavelength calibration error.

IV. EXPERIMENTAL APPARATUS AND OBSERVATIONS

A. Plasma source

Nitrogen plasmas were produced in the steady state, high density, helicon plasma source CHEWIE (the Compact Helicon Waves and Instabilities Experiment). The helicon source chamber is a 12 cm long, Pyrex tube, 6 cm in diameter, connected to a stainless steel expansion chamber, 30 cm long, and 15 cm in diameter (see Fig. 6). Vacuum pumping is accomplished with a rotary pump backed diffusion pump. After a base pressure of $\sim 10^{-7}$ Torr is attained, ultrahigh purity N_2 is fed into the system at the junction of plasma source-expansion chamber. A valve in front of the diffusion pump is then closed and a bypass valve opened to allow the rotary pump to pump directly on the plasma chamber. Thus, constant pressure (10–200 mTorr as measured by a thermocouple gauge calibrated with a Baratron gauge) with a variable gas flow rate (1–300 sccm) is achieved. A water-cooled electromagnet surrounds the source and is capable of generating a uniform axial magnetic field of 850 G in the source that rapidly diverges to nearly 0 G at the end of the expansion chamber (see Fig. 6). A 7 cm long, water cooled, Boswell saddle antenna[56] made from ¼ in. copper tubing couples the rf energy into the plasma through a Π-type matching network. rf power of up to 600 W is used to create the steady state plasma in the source chamber. To reduce the rf power radiated into the laboratory, a Faraday cage consisting of a copper mesh cover with a small aperture for the antennae feeds and water cooling lines and a 10 cm diam, 5 mm wall thickness copper tube is inserted between the antenna and the inside of the electromagnet (see Fig. 6). The rf driving frequency is typically set to the lower hybrid frequency[57]

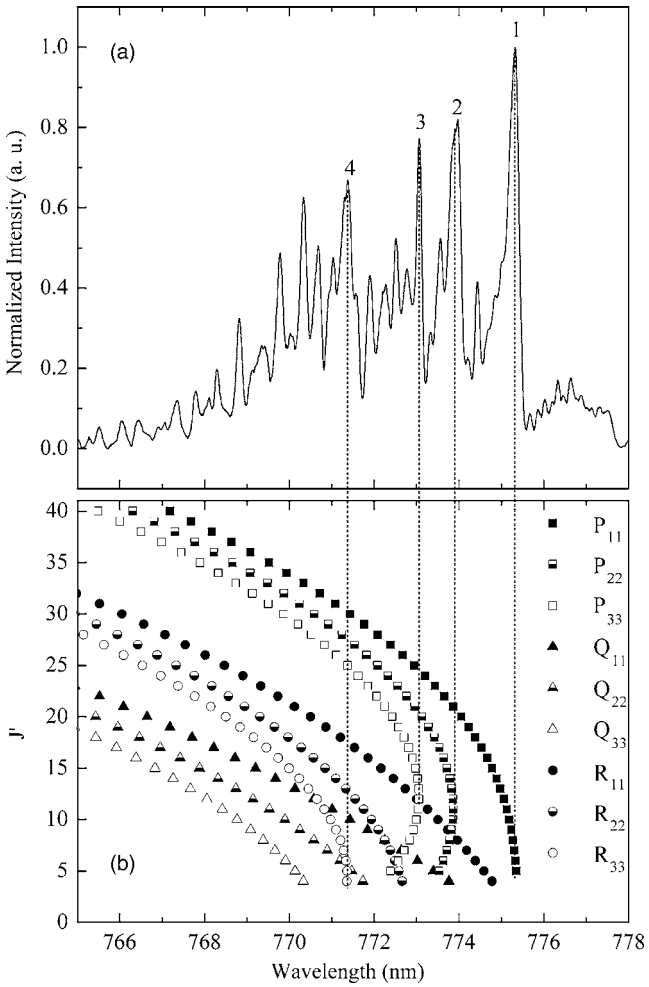

FIG. 4. The 2-0 band recorded spectrum (a) and corresponding Fortrat diagram (b); for simplicity, only the $(P,Q,R)_{ii}$ branches are plotted; the peaks 1–4 in the recorded spectrum correspond to the turning points of the P_{11}, P_{22}, P_{33}, and R_{33} branches.

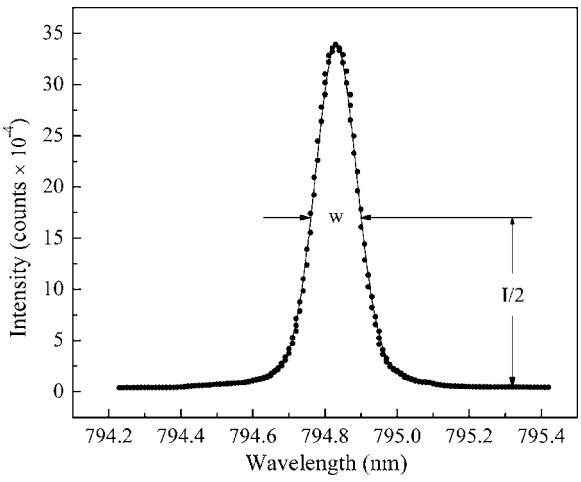

FIG. 5. A measured Ar I line calibration line at 794.818 nm (points) and corresponding fit (line) with the pseudo-Voight function given by Eq. (8).

TABLE III. Gauss-Lorentz relative contribution (p) and full width at half maximum (w) for Ar I lines used in the determination of the apparatus function.

Rotational band	λ (nm)	p	w (nm)
0→0	1047.005	0.37049	0.11066
1→0	912.297	0.26667	0.12669
	866.794		
2→0	794.818	0.24904	0.13901
	763.511		

$$\omega_{\mathrm{LH}}^{-1} \cong \sqrt{(\omega_{pi}^2+\omega_{ci}^2)^{-1}+(\omega_{ce}\omega_{ci})^{-1}}, \tag{10}$$

where ω_{ce}, ω_{ci} are the electron and ion cyclotron frequencies and ω_{pi} is the ion plasma frequency. For typical ion densities, the first term in Eq. (10) is negligible and $\omega_{\mathrm{LH}} \cong \sqrt{\omega_{ce}\omega_{ci}}$. Assuming a dissociation degree of 5% (Refs. 58 and 59) and that the ion population ratio (N^+/N_2^+) is the same as the dissociation degree, $f_{\mathrm{LH}} \approx 10.74$ MHz for a magnetic field of 850 G. Since the rf power was limited to 600 W, the E (capacitively coupled) and H (inductively coupled) modes were achieved in N_2 plasmas, but not the high density W mode (helicon mode).[60] For 10 mTorr at 80 sccm and a 0.88 W/cm^3 input power density in the E mode (the input power density was calculated by ignoring transmission losses after the matching network and taking the difference between forward and reflected power divided by the plasma source volume; if the expansion chamber volume is included, a power density of 53 mW/cm^3 is obtained), the plasma had a weak luminosity, low density of $n_e \approx 3\times10^{10}$ cm^{-3}, and a high electron temperature of $T_e \sim 5$ eV. In the H mode at double the input power density, the plasma had a strong (bright) luminosity, a slightly higher density $n_e \approx 8\times10^{10}$ cm^{-3} and a lower electron temperature, $T_e \sim 3$ eV as measured with a rf compensated Langmuir probe[61] 10 cm downstream in the expansion region.

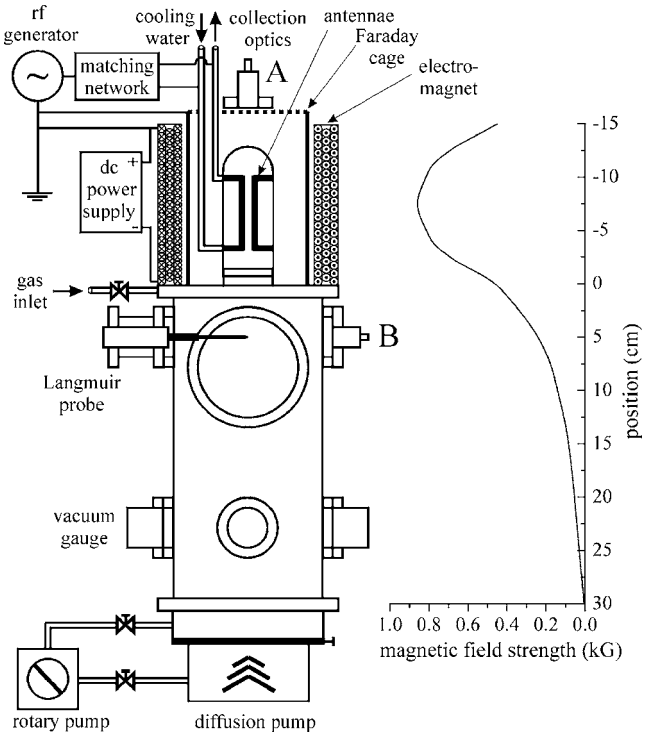

FIG. 6. Sketch of experimental arrangement (left) and the magnetic field profile (right) in CHEWIE plasma source-expansion chamber system.

B. Spectroscopic apparatus

The emission spectra were obtained with a 1.33 m Czerny-Turner double pass scanning monochromator (McPherson 209) with a 120×140 mm grating having 1200 tr/mm blazed at 750 nm. The linear dispersion of this system is 0.62 nm/mm and the maximum resolution is 0.015 nm. Scanning over the range 500–1100 nm is accomplished with a computer controlled stepper drive. The detector is an air cooled SBIG ST-7XEAI dual autofocusing CCD camera (Santa Barbara Instruments Group) having a 765×510 pixel array at 9 μm/pixel. The quantum efficiency of the camera is enhanced by the addition of a microlens array over the pixels. The quantum efficiency is 0.85 at 650 nm, ~0.45 toward the blue (400 nm) and ~0.05 toward the near-infrared (1000 nm). The acquisition time of the camera ranges from 10^{-2} to several hundred seconds. The camera has a high speed USB interface for PC data acquisition allowing transfer speeds of 1 frame/s. The light emitted by the helicon plasma source was focused by a series of 2.54 cm diam lenses into a 200 μm core multimode optical fiber and sent to the entrance slit of the monochromator.

Two spatial positions were used for light collection. One configuration has the collection optics close to the antenna and aligned axially with the discharge (position A in Fig. 6). In the second configuration the collection optics are aligned radially and light is collected through a radial viewport mounted on the expansion chamber (position B in Fig. 6). For all measurements reported here, the width of the entrance slit of the spectrometer was set to 80 μm and the integration time was chosen so that none of the bands intensities were saturated while still being long enough to measure the 0-0 band in near-infrared where the quantum efficiency of the CCD camera is poor. The entire optical path was calibrated in relative spectral response by using the tabulated spectral irradiance and the experimental measured spectrum of a tungsten ribbon lamp (Oriel^{TM}). Since the spectral window of the spectrometer-CCD camera system spans only 3.5 nm, the entire spectrum of each band was obtained through successive measurements in steps of 2 nm. The 1.5 nm overlap of adjacent measurements enabled reconstruction of the entire band spectrum by superimposing characteristic spectral features in the overlapping regions.

C. Gas temperature in a N_2 helicon plasma

Examples of measured rovibrational band spectra and the corresponding fits are shown in Figs. 7 and 8. As it can see, an excellent reproduction of the measured spectra is obtained for all three bands the confidence level being better than 95%. We believe that the small differences in intensities that appear between the numerically generated spectra and measured spectra are due to the change in spin orbit constant as J' increases and the Π_Ω manifolds change their character

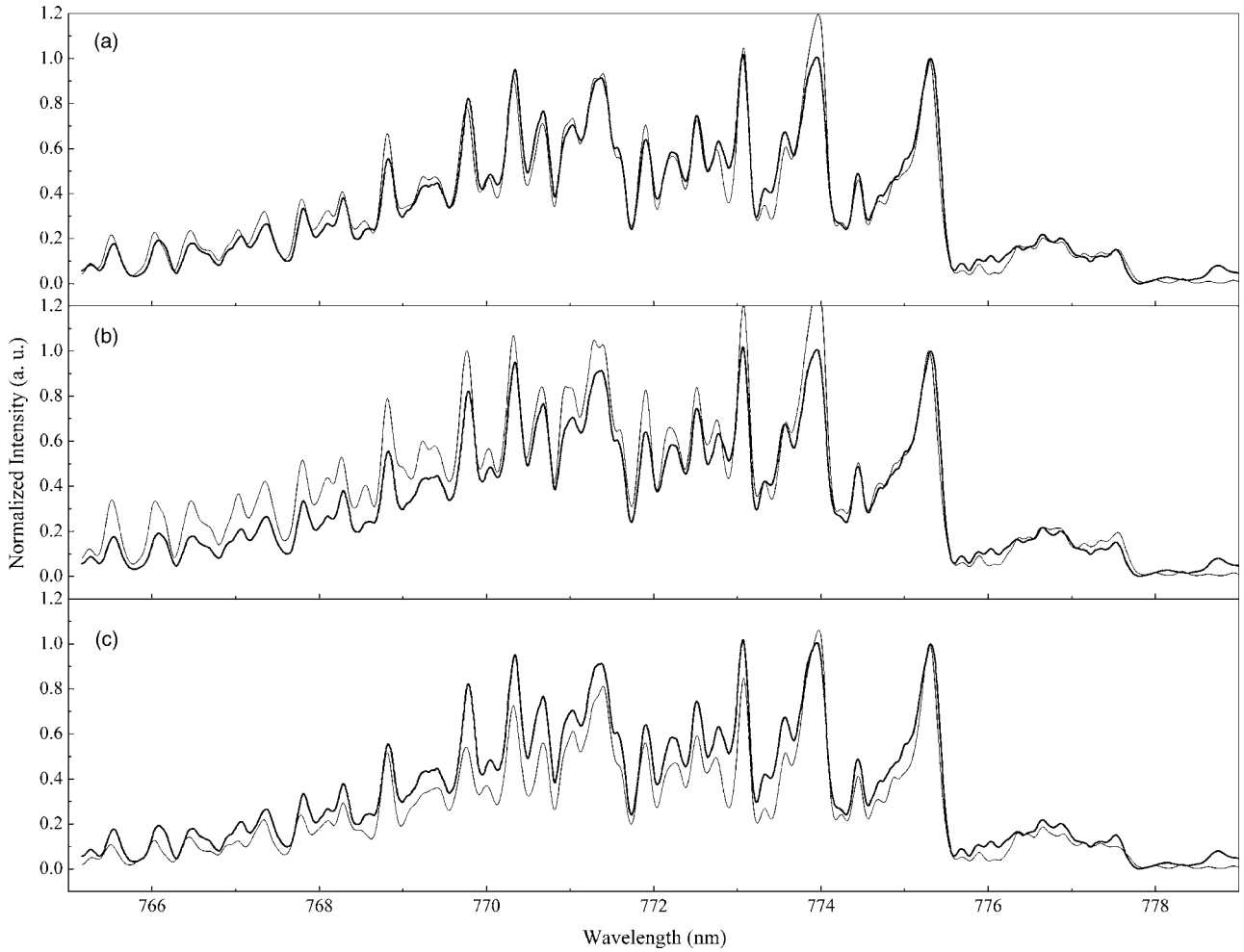

FIG. 7. (a) Experimental spectrum (thick line) and corresponding numerically generated spectrum (thin line) of the 2-0 band for the best fit gas temperature. To demonstrate the sensitivity of the fit to the gas temperature, experimental spectrum, and the numerical spectrum assuming a gas temperature (b) 100 K higher and (c) 100 K lower than the best fit temperature.

from Hund's case (a) toward case (b).[27] Table IV summarizes the gas temperatures obtained from fits to the measured spectra for different experimental conditions. The gas temperatures obtained from 2-0, 1-0, and 0-0 bands are mutually consistent and reasonable given the experimental conditions. For the sake of comparison, gas temperatures obtained by using the method of sub-band head intensity ratios (proposed by Simek and DeBenedictis[45]) are also listed in Table IV.

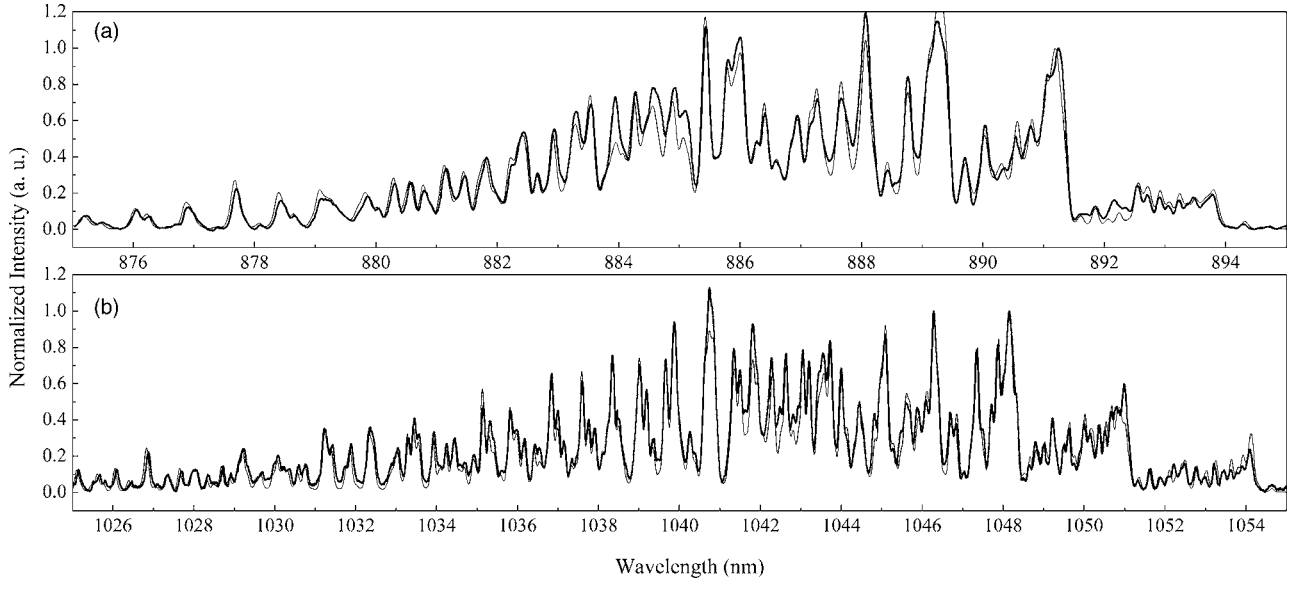

FIG. 8. Experimental spectra (thick line) and corresponding fits (thin line) of 1-0 band a), and 0-0 band b).

TABLE IV. Gas temperature obtained from the fit of 0-0, 1-0, and 2-0 bands and for comparison from peak ratio method from 3-0 band.

Working parameters and collection optics position	T_{gas} (K) from band fit				T_{gas} (K) from peak ratio[a]		
	$T_{2\to0}$	$T_{1\to0}$	$T_{0\to0}$	T_{fit}^{av}	T_{21}	T_{31}	T_{peak}^{av}
P=300 W, E-mode, radial collection	314±20	307±20	-	311±20	296±25	308±25	302±25
P=300 W, E-mode, axial collection	360±22	372±23	-	366±23	341±25	373±25	357±25
P=600 W, H-mode, radial collection	391±24	407±25	398±24	399±24	371±25	392±25	381±25
P=600 W, H-mode, axial collection	486±28	502±29	508±29	499±29	446±25	499±25	473±25

[a]As described in Ref. 45.

The agreement between our spectral fitting method and the Simek and DeBenedictis method is also very good. Thus, it appears that for the $v=0-3$ vibrational levels, the rotational distributions are thermalized. Preliminary investigation of the vibrational distributions show a slight decrease (from ~6700 to ~6200 K) in the vibrational temperature as rotational temperature increases from 310 to 500 K. Although a complete analysis of the gas temperature in a helicon plasma is beyond the scope of this article, we note some particularly striking features in our initial observations. First, from the inferred T_g values there appears to be a significant temperature gradient along the discharge axis for E mode (2.5 K/cm) that becomes even steeper in the H mode (5 K/cm). Since the plasma is produced in the gas volume surrounded by the antennae, and due to divergent magnetic field geometry (the magnetic field strength drops from 850 G in the source to 140 G on the axis at the observation point B), this observation is consistent with cooling of hotter gas molecules in the higher confinement source region by inelastic collisions with colder gas molecules injected at the source-expansion chamber junction. An important caveat is that since optical emission spectroscopy provides a line-of-sight averaged measurement, the axially averaged measurements obtained at location A (Fig. 6) are the on-axis gas temperatures but the measurements obtained at location B are radially averaged gas temperature measurements. If we assume that gas heating occurs only through electron-driven processes,[12] it is reasonable to assume that for the cylindrical geometry of this experiment the radial gas temperature distribution tracks the radial electron density distribution. Using the simple Schottky model for radial ambipolar diffusion,[62] it follows that

$$T_g(r) = T_{wall} + (T_{on\text{-}axis} - T_{wall})J_0(2.405r/R), \tag{11}$$

where J_0 is the zeroth order Bessel function and R the chamber radius. In the absence of ion heating of the gas, ignoring any gas thermal conductivity dependence on temperature or pressure and in the absence of cold gas, the radial gas temperature profile should be peaked on axis. Thus, the line-of-sight averaged gas temperature when measured radially would be lower than measured axially. Detailed measurements of the gas temperature radial profile are planned to determine if our initial observations of a strong axial gas temperature gradient could result from radial temperature profile effects.

Another interesting initial result is that the gas temperature is higher in the inductively coupled regime than capacitively coupled regime. This observation is most likely explained by improved efficiency in coupling the rf power into the discharge in the H mode compared to the E mode.[63] Donnelly and Malyshev[12] have reported gas temperatures close to the wall temperature (300 K) for a 13.56 MHz, $Cl_2+5\%N_2$, 20 mTorr discharge in E mode and temperatures as high as 1250 K in H mode, for a 0.36 W/cm^3 power density. The quite high gas temperature in the later case was explained by efficient gas heating through energy released by electron dissociation of the Cl_2 molecule.

V. SUMMARY

The gas temperature measurement technique described in this work employs fits to detailed spectroscopic measurements of the 0-0, 1-0, and 2-0 emission bands of the first positive system of N_2. The fitting code along user instructions is available for download from Electronic Physics Auxiliary Publication Service (EPAPS)[64] and West Virginia University Helicon Plasma Group website.[65] The code includes the line positions and Hönl-London factors for all three bands. Since the apparatus function is an input to the fitting code, the analysis can be performed with either high or low resolution spectrometers. Initial tests of the technique obtained nearly identical results when any of the three bands of the first positive system were used in the analysis.

An accurate determination of gas temperature using this analysis technique requires:

1. A measurement of the spectrum of one or more of the three bands.
2. Determination of the parameters p and w for the spectrometer by using a low temperature lamp to record a spectral line in the relevant spectral range that is then fit with Eq. (8).
3. Use of a standard intensity calibration lamp to correct for the optical system wavelength sensitivity.
4. Analysis of the band spectra with the MATLAB™ code.

[1]J. Fandiño, G. Santana, L. Rodríquez-Fernández, C. Cheong-Wong, A. Ortiz, and J. C. Alonso, J. Vac. Sci. Technol. A **23**, 248 (2005).
[2]C. Muratore, S. G. Walton, D. Leonhardt, and R. F. Fernsler J. Vac. Sci. Technol. A **24**, 25 (2006).
[3]R. Fu, X. Tian, and P. Chu, Rev. Sci. Instrum. **74**, 3697 (2003).
[4]R. F. Boivin and E. E. Scime, Plasma Sources Sci. Technol. **14**, 283 (2005).

[5]G. Gardet, G. Mailard, M. Courbon, F. Rogemond, and M. Oruetta, Meas. Sci. Technol. **11**, 333 (2000).
[6]N. K. Bibinov, A. Fateev, and K. Wiesemann, Plasma Sources Sci. Technol. **10**, 579 (2001).
[7]V. Linss, H. Kupfer, S. Peter, and F. Richter, J. Phys. D **37**, 1935 (2004).
[8]J. M. Williamson and C. A. DeJoseph, Jr., J. Appl. Phys. **93**, 1893 (2003).
[9]H. Nassar, S. Pellerin, K. Musiol, O. Martinie, N. Pellerin, and J-M. Cormier, J. Phys. D **37**, 1904 (2004).
[10]M. Tuszewski, J. Appl. Phys. **100**, 053301 (2006).
[11]G. P. Davis and R. Gottscho, J. Appl. Phys. **54**, 3080 (1983).
[12]V. M. Donnelly and M. V. Malyshev, Appl. Phys. Lett. **77**, 2467 (2000).
[13]E. J. Tonnis and D. B. Graves, J. Vac. Sci. Technol. A **20**, 1787 (2002).
[14]B. Bai, H. Sawin, and B. Cruden, J. Appl. Phys. **99**, 013308 (2006).
[15]F. Iza and J. A. Hopwood, IEEE Trans. Plasma Sci. **32**, 498 (2004).
[16]G. Faure and S. M. Shkol'nik, J. Phys. D **31**, 1212 (1998).
[17]B. A. Cruden, M. V. V. S. Rao, S. P. Sharma, and M. Meyyappan, J. Appl. Phys. **91**, 8955 (2002).
[18]N. Goyette, J. R. Peck, Y. Matsuda, L. W. Anderson, and J. E. Lawler, J. Phys. D **31**, 1556 (1998).
[19]Yu. B. Golubovskii and V. M. Telezhko, J. Appl. Spectrosc. **39**, 999 (1983).
[20]S. Kado *et al.*, J. Plasma Fusion Res. **7**, 54 (2006).
[21]B. P. Lavrov, M. Osiac, A. V. Pipa, and J. Ropke, Plasma Sources Sci. Technol. **12**, 576 (2003).
[22]M. Shimada, R. Cattolica, and G. R. Tynan, J. Vac. Sci. Technol. A **22**, 371 (2004).
[23]B. Bakowski, G. Hancock, R. Peverall, G. A. D. Ritchie, and L. J. Thornton, J. Phys. D **37**, 2064 (2004).
[24]C. Foissac, A. Campargue, A. Kachanov, P. Suipiot, G. Weirauch, and N. Sadeghi, J. Phys. D **33**, 2434 (2000).
[25]M. Simek, G. Dilecce, and S. De Benedictis, Plasma Chem. Plasma Process. **15**, 427 (1995).
[26]A. Lofthus and P. Krupenie, J. Phys. Chem. Ref. Data **6**, 115 (1977).
[27]G. Herzberg, *Molecular Spectra and Molecular Structure. I. Spectra of Diatomic Molecules* (Krieger, Malabar, FL, 1989).
[28]M. Alexander and B. Pouilly, J. Chem. Phys. **79**, 1545 (1983).
[29]S. DeBenedictis, G. Dilecce, and M. Simek, J. Chem. Phys. **110**, 2947 (1999).
[30]D. C. Cartwright, S. Trajmar, A. Chutjian, and W. Williams, Phys. Rev. A **16**, 1041 (1977).
[31]D. C. Cartwright, J. Appl. Phys. **49**, 3855 (1978).
[32]J. S. Morrill, W. M. Benesch, and K. G. Widing, J. Chem. Phys. **94**, 262 (1991).
[33]B. Krames Th. Glenewinkel-Meyer, and J. Meichsner, J. Phys. D **34**, 1789 (2001).
[34]P. Supiot, D. Blois, S. De Benedictis, G. Dilecce, M. Barj, A. Chapput, O. Dessaux, and P. Goudmand, J. Phys. D **32**, 1887 (1999).
[35]L. G. Piper, K. W. Holtzclaw, B. D. Green, and W. A. M. Blumberg, J. Chem. Phys. **90**, 5337 (1989).
[36]A. V. Phelps, J. Phys. Chem. Ref. Data **20**, 557 (1991).
[37]E. W. McDaniel, *Collision Phenomena in Ionised Gases* (Wiley, New York, 1964), Vol. I.
[38]H. J. Werner, J. Kalcher, and E. A. Reinsch, J. Chem. Phys. **81**, 2420 (1984).
[39]L. G. Piper, J. Chem. Phys. **88**, 6911 (1988).
[40]B. Krames Th. Glenewinkel-Meyer, and J. Meichsner, J. Appl. Phys. **89**, 3115 (2001).
[41]H. Geisen, D. Neuschafer, and Ch. Ottinger, J. Chem. Phys. **92**, 104 (1990).
[42]E. E. Eyler and F. M. Pipkin, J. Chem. Phys. **79**, 3654 (1983).
[43]NIST atomic spectral lines database, www.nist.gov
[44]R. P. Vaudo, J. W. Cook, Jr., and J. F. Schetzina, J. Vac. Sci. Technol. B **12**, 1232 (1994).
[45]M. Simek and S. De Benedictis, Plasma Chem. Plasma Process. **15**, 451 (1995).
[46]A. Ricard, C. Nouvellon, S. Konstantinidis, J. P. Dauchot, M. Wautelet, and M. Hecq, J. Vac. Sci. Technol. A **20**, 1488 (2002).
[47]A. Budo, Z. Phys. **105**, 73 (1937).
[48]J. L. Dunham, Phys. Rev. **41**, 721 (1932).
[49]C. Effantin, C. Amiot, and J. Verges, J. Mol. Spectrosc. **76**, 221 (1979).
[50]P. E. Ciddor, Appl. Opt. **35**, 1566 (1996).
[51]A. Schadee, Astron. Astrophys. **14**, 401 (1971).
[52]C. O. Laux and C. H. Kruger, J. Quant. Spectrosc. Radiat. Transf. **48**, 9 (1992).
[53]J. B. Tatum, Astrophys. J., Suppl. Ser. **14**, 21 (1967).
[54]I. Kovacs, *Rotational Structure in the Spectra of Diatomic Molecules* (American Elsevier, New York, 1969).
[55]F. Roux, F. Michaud, and J. Verges, J. Mol. Spectrosc. **97**, 253 (1983).
[56]R. W. Boswell, Phys. Lett. **33A**, 457 (1970).
[57]J. L. Kline, E. E. Scime, R. F. Boivin, A. M. Keesee, X. Sun, and V. S. Mikhailenko, Phys. Rev. Lett. **88**, 195002 (2002).
[58]T. Czerwiec, F. Greer, and D. B. Graves, J. Phys. D **38**, 4278 (2005).
[59]T. Nakano, S. Kumagai, and S. Samukawa, J. Appl. Phys. **92**, 2990 (2002).
[60]V. Kaeppelin, M. Carrere, and J. B. Faure, Rev. Sci. Instrum. **72**, 4377 (2001).
[61]C. Biloiu, E. Scime, X. Sun, and B. McGeehan, Rev. Sci. Instrum. **75**, 4296 (2004).
[62]W. Schottky, Z. Phys. **25**, 635 (1924).
[63]K. N. Ostrikov, S. Xu, and S. Azam, J. Vac. Sci. Technol. A **20**, 251 (2002).
[64]See EPAPS Document No. E-JAPIAU-101-080704 for the fitting code along with line positions and intensities. This document can be reached through a direct link in the online article's HTML reference section or via the EPAPS homepage (http://www.aip.org/pubservs/epaps.html).
[65]West Virginia University Helicon Plasma Group, http://ulysses.phys.wvu.edu/~plasma/